Combustion and Flame 284 (2026) 114665

Contents lists available at ScienceDirect

Combustion and Flame

journal homepage: www.sciencedirect.com/journal/combustion-and-flame

Extinction characteristics of laminar bluff body flames in a transverse direct current electric field

Bowen Liu [a], Jianling Li [b], Yunke Wu [c,*], Hao Zhao [a,*]

[a] School of Mechanics and Engineering Science, Peking University, Beijing 100871, China
[b] School of Power and Energy, Northwestern Polytechnical University, Xi'an 710072, China
[c] Aero Engine Corporation of China, Beijing 101399, China

ARTICLE INFO

Keywords:
Direct current
Transverse electric field
Bluff body flames
Extinction
Thermal diffusive instability

ABSTRACT

The effect of the transverse direct current (DC) electric field on bluff body flames was investigated across four flame morphologies, such as attachment, partial attachment, lifting, and blow out in experiments by using a $CH_4/O_2/N_2$ mixture with equivalence ratios (ϕ) ranging from 0.55 to 0.90 at a constant flow velocity ($V = 1$ m/s). The high-intensity transverse DC electric field accelerated the transition between flame morphologies, from attachment to partial attachment, then to lifting, and finally to blow out (extinction), primarily due to the effect of ionic wind. Further, the extinction induced by the transverse DC electric field was explored in terms of the flame instability by using a $CH_4/O_2/CO_2/N_2$ mixture with different Lewis numbers (*Le*). Under a transverse DC electric field with a bias voltage of 4 kV, visible flame distortions caused by thermal diffusive instabilities were observed in the $CH_4/O_2/CO_2/N_2$ mixture at $\phi = 0.55$, $V = 1$ m/s, and $Le \approx 1.0$, which were not observed without the electric field. Meanwhile, the bias voltage required for extinguishing bluff body flames decreased at a larger blending ratio of CO_2 or a lower Lewis number. The results indicated that the transverse DC field led to an early flame extinction through both the ionic wind effects and exacerbated thermal diffusive instability.

1. Introduction

The electric field generated by the potential difference has gained significant attention from researchers as a non-invasive means of the combustion modulation [1,2]. Numerous studies have showcased the influence of electric fields on the flame stabilization [3–6], pollutant control [7], and combustion enhancement [8,9]. The effects of different configurations of electric fields, such as transverse [10], longitudinal [11,12], and single electrode [13] electric fields generated by direct current (DC) [14,15] or alternating current (AC) [9,16–21] sources have been studied on different types of flames, including spherical propagating flames [8,9], Bunsen flames [4,11,22,23], flat flames [15,24], counterflow diffusion flames [20,25,26], and jet flames [5,6,10,14].

Recent studies primarily focus on the impact of DC electric fields on the flammability limits of flames [4–6,19,27–29], flame speed, temperature, and instabilities [11,30–32]. For example, Noorani et al. [6] examined the effect of the DC electric field on the blowout limit of CH_4/air jet flames. The results indicate that with a specific electrode configuration, a longitudinal DC electric field enhances flame stability, with the positive electrode placed horizontally above the flame and the negative electrode connected to the burner. In contrast, a transverse electric field does not show significant effects due to the severe flame stretching. Wisman et al. [11] investigated the effect of a longitudinal DC electric field on the stability of premixed C_3H_8/air flames. It is shown that a stable conical flame can transition to a wrinkled laminar flamelet and further develop into a highly unstable distributed flamelet regime or collective flame front oscillations at appropriate electrode geometries and applied voltages. Mario et al. [32] developed a one-dimensional premixed flame model, revealing that positive electric fields accelerate electron accumulation in low-temperature regions, boosting the exothermic recombination of ionized products and significantly increasing flame speed. Similarly, Vega et al. [31] found that high-strength DC electric fields induce flame surface deformation in CH_4/air laminar flames, altering flame speed and temperature through ionic wind-enhanced flame stretch. Most of these works have concentrated on longitudinal DC electric fields, where ionic wind induces bulk flow acceleration or deceleration, thereby modifying flame stretch and triggering flame instabilities that ultimately lead to either enhanced flames or extinction. In contrast, the ionic wind generated by transverse DC electric fields acts perpendicular to the main flow direction, resulting

* Corresponding authors.
E-mail addresses: buaaake@buaa.edu.cn (Y. Wu), h.zhao@pku.edu.cn (H. Zhao).

https://doi.org/10.1016/j.combustflame.2025.114665
Received 24 February 2025; Received in revised form 19 November 2025; Accepted 20 November 2025
Available online 26 November 2025

in asymmetric flame deflection and localized flow perturbation rather than uniform bulk acceleration. However, there is a noticeable lack of comprehensive investigations on the effects of transverse electric fields. Furthermore, while prior research attributes electric field-induced flame instabilities primarily to ionic wind and its impact on flame stretch and speed, highlight a significant gap in understanding the intrinsic flame instabilities [33–37] (such as hydrodynamic and thermal diffusive instabilities) governing extinctions. While hydrodynamic instabilities are prominent in turbulent or high-velocity flows [38], thermal diffusive instabilities, driven by the preferential diffusion of mass versus heat, become significant in laminar lean flames near flammability limits, leading to flame front wrinkles, distortions, and cellular structures [39, 40]. Meanwhile, the thermal diffusive instability gets significant at lower equivalence ratios or flame temperatures [41]. Wisman et al. [11] observed that longitudinal DC electric fields exacerbate thermal diffusive instabilities, but the role of transverse DC electric fields in inducing such instabilities and extinctions remains underexplored.

The objective of this study is to investigate the morphology and extinction characteristics of bluff body flames under the influence of a transverse DC electric field, with a specific focus on elucidating the physical mechanisms driving flame extinction. Specifically, the research aims to: (i) classify flame morphologies, including attachment, partial attachment, lifting, and blowout, and analyze their transitions under varying transverse DC electric field conditions through experimental analysis; (ii) investigate the role of thermal diffusive instabilities in CO_2-diluted flames with different Lewis numbers (*Le*) to uncover the intrinsic dynamic mechanisms governing electric field-controlled flame instabilities and extinction. This work is crucial for advancing electric field based fire suppression technologies [42,43] and optimizing combustion in various engineering applications [9,44,45].

2. Methods

2.1. Experimental methods

A transverse DC electric field was arranged in a bluff body burner of laminar premixed flames, as is shown in Fig. 1. The fuel and air gases were premixed in an upstream cavity and passed through a ceramic honeycomb filter for rectification. The bluff body burner was constructed using high-temperature resistant ceramics as materials. Fig. 1 (a) illustrate the electric field configuration. A transverse DC electric field was generated between the two stainless steel plate electrodes with dimensions of 60 mm in length, 30 mm in width, and 5 mm in thickness. The distance between the two plate electrodes was 50 mm. Two quartz windows were symmetrically positioned at the front and back to enable flame observation. A conical bluff body was installed at the burner inlet to stabilize the flames, as is shown in Fig. 1(b). The bluff body was connected to the ceramic seat via a female thread. To hold the center bluff body stationary, the center block of the ceramic seat was attached to the outer annulus using six equally spaced thin plates of 0.8 mm thickness. As a result, the premixed gas was divided to form a flap-shaped flame. The outer and inner diameters of the annular inlet were 20 mm and 15 mm, respectively. The velocity of the inlet flow, *V*, was defined as the ratio of the volume flow rate to the inlet cross-sectional area. In this work, the fluid motion was considered to be laminar and the range of Reynolds numbers, *Re*, for all conditions was <400.

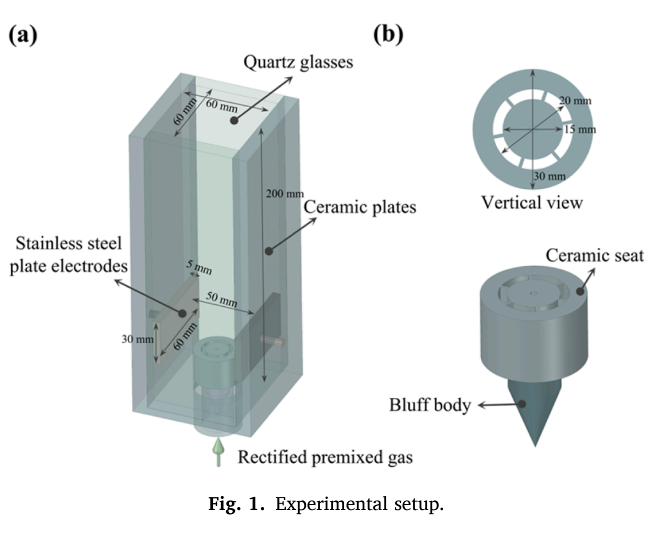

Fig. 1. Experimental setup.

The morphology of flames was recorded using a high-speed image enhancement camera (FASTCAM SA-Z combined with Invisible Vision UVi) with a sampling frame rate of 2000 FPS and exposure time of 400 μs. To assess localized quenching, regions of the flame exhibiting reduced reactivity were identified in the captured flame images. Specifically, localized quenching was determined by defining areas where the intensity was <3 % of the maximum intensity observed in the flame images as quenched regions. Spectrally resolved images of chemically excited flame radicals, CH* and OH*, were also recorded utilizing narrow bandpass (10 nm) interference filters (431 nm and 307 nm). A high-voltage DC source (Teslaman TLP2041) with a maximum voltage of 10 kV was used as an excitation device for the transverse electric field. To measure the ionic current (*I*) induced by the electric field, a micro-ammeter (resolution of 0.1 μA) was connected in series within the circuit. A high energy igniter was utilized for the ignition of the mixture, which was accomplished by inserting two tungsten electrodes into the combustion chamber. Particle Image Velocimetry (PIV) measurements were conducted using a PIV system (LaVision) equipped with a double-pulsed Nd:YAG laser operating at a wavelength of 532 nm to investigate the velocity field of the flame under the transverse DC electric field. This system enabled detailed characterization of the flow field, particularly highlighting the effects of the ionic wind on the velocity distribution near the electrodes and the bluff-body. The flow of gases during experiments was precisely controlled by mass flow controllers (Brooks GF125) with an accuracy of ± 0.5 % of the full scale. The air was configured from 21 % and 79 % volume fractions of oxygen and nitrogen, respectively. The purity of gases in this work exceeded 99.999 %. The equivalence ratio (ϕ) can be calculated by:

$$\phi = \frac{\left(N_{O_2}/N_{fuel}\right)_{stoichiometric}}{\left(N_{O_2}/N_{fuel}\right)_{actual}} \tag{1}$$

where$N_{fuel}$and N_{O_2}represent the mole fraction of fuel and oxygen, respectively.

The thermal diffusive instability of the mixture is characterized by the Lewis number (*Le*), which is defined as:

$$Le = \frac{D_{th}}{D_m} = \frac{\lambda}{\rho c_p D_m} \tag{2}$$

where D_{th}, D_m, λ, ρ, and c_p represent the thermal and mass diffusivity coefficients, thermal conductivity, density, and specific heat capacity, respectively. Specifically, thermal conductivity (λ) and specific heat capacity (c_p) are calculated using mass fraction weighted averaging of individual species conductivities. Density (ρ) obtained from ideal gas law. The mass diffusivity coefficient (D_m) is calculated using the mixture-averaged method and the target component (fuel under fuel-lean condition) [46] diffusion coefficient ($D_{f,m}$) is given in terms of the binary diffusion coefficients [47].

$$D_m = D_{fuel} = D_{f,m} = \frac{1 - Y_f}{\sum_{i \neq f}^{n} X_i \Big/ D_{f,i}} \tag{3}$$

where Y_f, X_i, and $D_{f,i}$ represent the mass fraction of fuel, the mole fraction of specie *i*, and the binary diffusion coefficient between fuel and specie *i*, respectively. The *Le* of the mixture can be adjusted by blending diluent gases, such as CO_2, Ar and He. In this work, the *Le* of the premixed gas is reduced by blending CO_2.The blending ratio of CO_2 (x) can be calculated by:

$$x = \frac{X_{CO_2}}{X_{CO_2} + X_{N_2}} \tag{4}$$

where X_{CO_2} and X_{N_2}represent the mole fraction of CO_2 and N_2 in the mixture, respectively. To maintain the adiabatic flame temperature unaffected, the dilution gas scaling factor, β, is involved. The adiabatic flame temperature and laminar burning velocity are calculated by Cantera in this work. The composition of the new mixture is as follows:

$$CH_4 + O_2 + \beta[(1-x)N_2 + xCO_2] \tag{5}$$

2.2. Electrostatic field computation

The two-dimensional electrostatic field was calculated using the ANSOFT Maxwell 14.0 software to characterize the electric field distribution generated by the transverse electrodes. The electric field computation is performed using a 2D computational domain (600 mm × 600 mm) that encompasses the burner geometry and surrounding region. The domain is designed to capture the electric field distribution in the combustion zone while ensuring that boundary effects do not influence the solution in the region of interest. The computational domain extends sufficiently beyond the burner to allow for proper boundary condition application and field decay. Maxwell 14.0 employs the electrostatic approximation rather than solving the full time-dependent Maxwell equations. The boundary conditions applied include Dirichlet boundary conditions on the electrode surfaces with specified potential values corresponding to the applied voltage, and the far-field boundaries to simulate infinite domain conditions. As was shown in Fig. 2, under the bias voltage (U_{bias}) of 5 kV, a unidirectional electric field which is in the direction of the positive electrode towards the negative electrode is generated. The distribution of the strength of the electric field exhibits symmetry about the central plane between the electrodes. The flame is considered as a “weak plasma” characterized by a low ionization degree [1,8,17], with charge carriers in the reaction zone that cause only minimal perturbations to the uniformity of the electric field. Due to the low conductivity and weak ionization of flame, the use of electrostatic field modeling is appropriate, ensuring that the applied electrode voltage governs the overall field distribution. As such, the magnitude of the voltage bias is employed to provide a qualitative description of the electric field strength.

3. Results and discussion

3.1. The morphology and flow field of bluff body flames

All of the inlet flows are laminar under the present conditions. The four regions of the flame morphologies for the CH_4/air flame at different equivalence ratios (ϕ) and flow velocities (V) without and with an applied electric field are depicted in Fig. 3(a) and Fig. 3(b). At a fixed V,

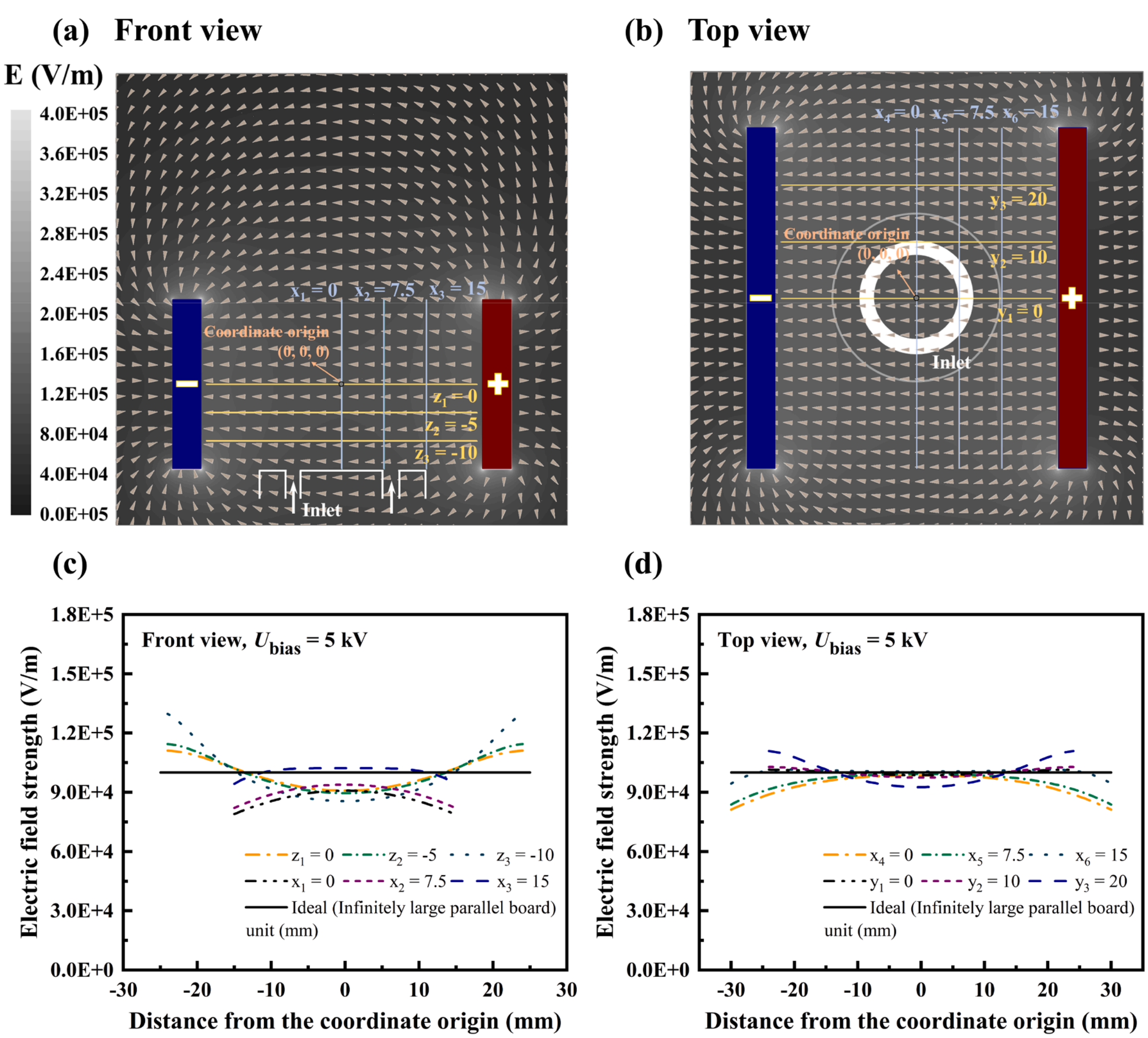

Fig. 2. Vector and strength distribution of the transverse DC electric field (U_{bias} = 5 kV).

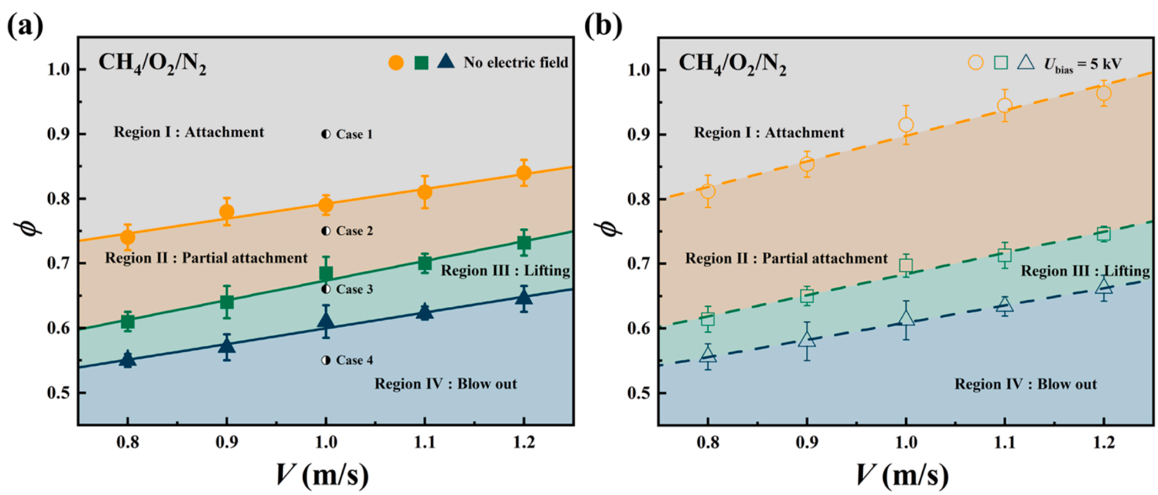

Fig. 3. The sub-area map of the morphology of the bluff body flames with and without an applied electric field. (a) $U_{\text{bias}} = 0$ kV; (b) $U_{\text{bias}} = 5$ kV.

the morphology of flames transitions from attachments, to partial attachments, then to lifting, and finally to blow out (extinctions) as ϕ decreases. Under the present conditions, the critical ϕ for the transitions between the different morphologies of bluff body flames can be fitted approximately linearly over different V in Fig. 3. It is found that there is no significant effect of the transverse DC electric field on the flammable limit under $U_{\text{bias}} = 5$ kV, with the ideal electric field strength of 10,000 V/m. Similarly, Noorani et al. [6] also mentioned that the transverse DC electric field did not contribute to the broadening of the flammable limit and stabilities in the CH_4/air jet flames. However, the electric field significantly influences the transition from attached to partially attached morphologies, shifting the transition line to higher ϕ and lower V, as is shown in Fig. 3(b). This indicates that the electric field promotes flame detachment from the burner. The typical morphology of CH_4/air flames could be clearly distinguished under $V = 1$ m/s, as is shown in Fig. 4. The fresh premixed gas is split due to the inlet morphology of the burner, resulting in a flap-shaped flame captured by the high-speed camera, which has been illustrated in the experimental methods. As to attached flames, the bottom border of flames sits on the burner exit, while for partial attachment, the outer edge of flames detaches from the burner. Under the lifting morphology, the bottom of bluff body flames is fully blown off from the burner exit. The blow out of bluff body flames occurs with a further decrease of ϕ and the entire visible field is in darkness.

Fig. 5 presents a comparative analysis of the flow field characteristics of bluff body flames without and with the transverse DC electric field ($U_{\text{bias}} = 8$ kV) at $\phi = 0.90$ and $V = 1$ m/s. In the baseline condition without electric field (Fig. 5(a)), the flow field exhibits a symmetric wake structure typical of bluff body stabilized flames. When a transverse DC electric field is applied, the flow field undergoes significant asymmetry, deflecting markedly toward the negative electrode as depicted in Fig. 5(b). Near this electrode, the flow accelerates notably, driven by electrohydrodynamic (EHD) forces arising from interactions between the electric field and charged species in the combustion environment. The ionic wind effect, induced by the motion of charged particles, imparts additional momentum, enhancing local flow velocity near the negative electrode. Additionally, the flow field discontinuity observed at the edges of the viewing window under the electric field is attributed to insufficient particle density in these regions, leading to divergent flow velocity calculations.

3.2. The effects of the transverse DC electric field on flame morphologies

The interactions between electric fields and flames have been extensively studied and are primarily attributed to ionic wind. The charge carriers, generated primarily through the chemical ionization in the reaction zone of a flame [1], are accelerated by electric fields. The positive ions migrate toward the negative electrode, while the negative ions and electrons migrate toward the positive electrode. Negative ions are unstable and quickly decay into electrons and neutral molecules at high temperatures [48], while electrons have a negligible mass. Therefore, positive ions dominate the momentum transfer and mass diffusion in the ionic wind. The collisions and reactions between accelerated ions and molecules, as are suggested by existing literature [1,2], may influence both the flame morphology and luminescence, though these effects have not been directly measured in the present study. To explore the effect of the transverse DC electric field on the morphology and structure

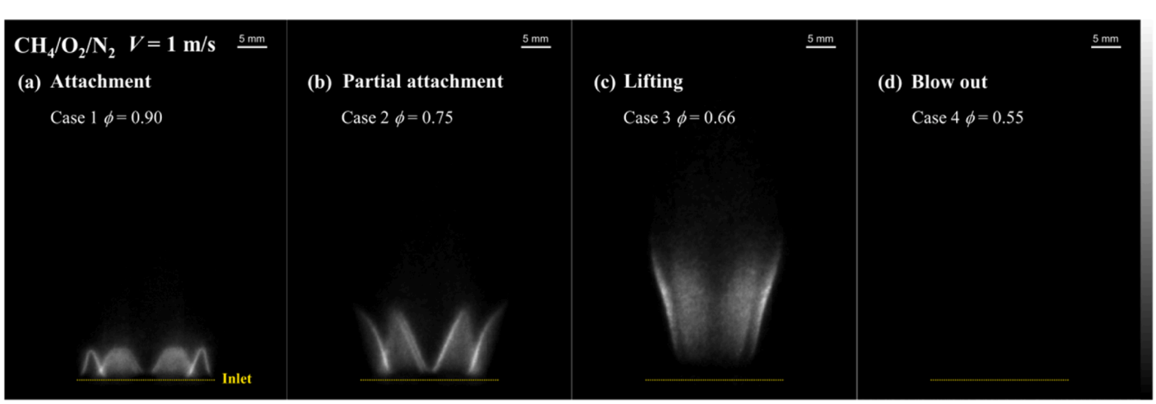

Fig. 4. Direct high-speed images of bluff body flames corresponding to the typical regions. (a) $\phi = 0.90$; (b) $\phi = 0.75$; (c) $\phi = 0.66$; (d) $\phi = 0.55$.

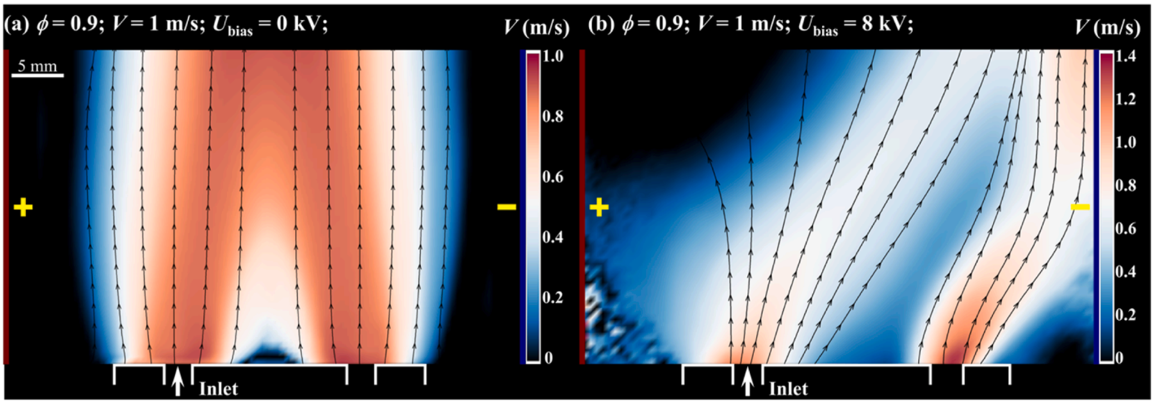

Fig. 5. Time-averaged flow field of bluff body flames without and with an applied electric field at ϕ = 0.90 and V = 1 m/s. (a) U_{bias} = 0 kV; (b) U_{bias} = 8 kV.

of bluff body flames, three typical conditions at V = 1 m/s in flame morphologies of attachment (ϕ = 0.90), partial attachment (ϕ = 0.75), and lifting (ϕ = 0.66), as is classified in Fig. 6, are investigated in a transverse DC electric field with varied voltage. The specific experimental conditions are detailed in Table 1.

The effect of a transverse DC electric field on the morphology of bluff body flames is shown in Fig. 6. It is seen that the effects of the transverse DC electric field on the flame morphology of attachment, partial attachment, and lifting are similar, where the effect is negligible at U_{bias} ≤ 2 kV. With U_{bias} or the electric field strength increasing, the flame deflects towards the negative electrode, which is evident from the images of the enhanced shaded areas at U_{bias} = 0 kV and 8 kV, as is shown in Fig. 6(a). This deflection is mainly due to the movement of positive ions in the ionic wind towards the negative electrode. Notably, the flame transits from attachment to partial attachment on the left side close to the negative electrode at U_{bias} ≥ 6 kV. One of the possible reasons for the transition in the morphology of bluff body flames is the enhancement of flow velocities due to the ionic wind, which is more significant near the negative side, as shown in Fig. 5 [49]. In the case of partial attachment flames at ϕ = 0.75, similarly, flames deflect to the left side and the flap-shaped flames are more concentrated near the negative electrode

Table 1
Experimental conditions under the transverse DC electric field.

Mixture	V (m/s)	ϕ	U_{bias} (kV)	T_a (K)	S_L (cm/s)
$CH_4/O_2/N_2$	1	0.90	0 - 10	2139.1	33.8
$CH_4/O_2/N_2$	1	0.75	0 - 10	1924.9	24.4
$CH_4/O_2/N_2$	1	0.66	0 - 10	1775.1	16.9

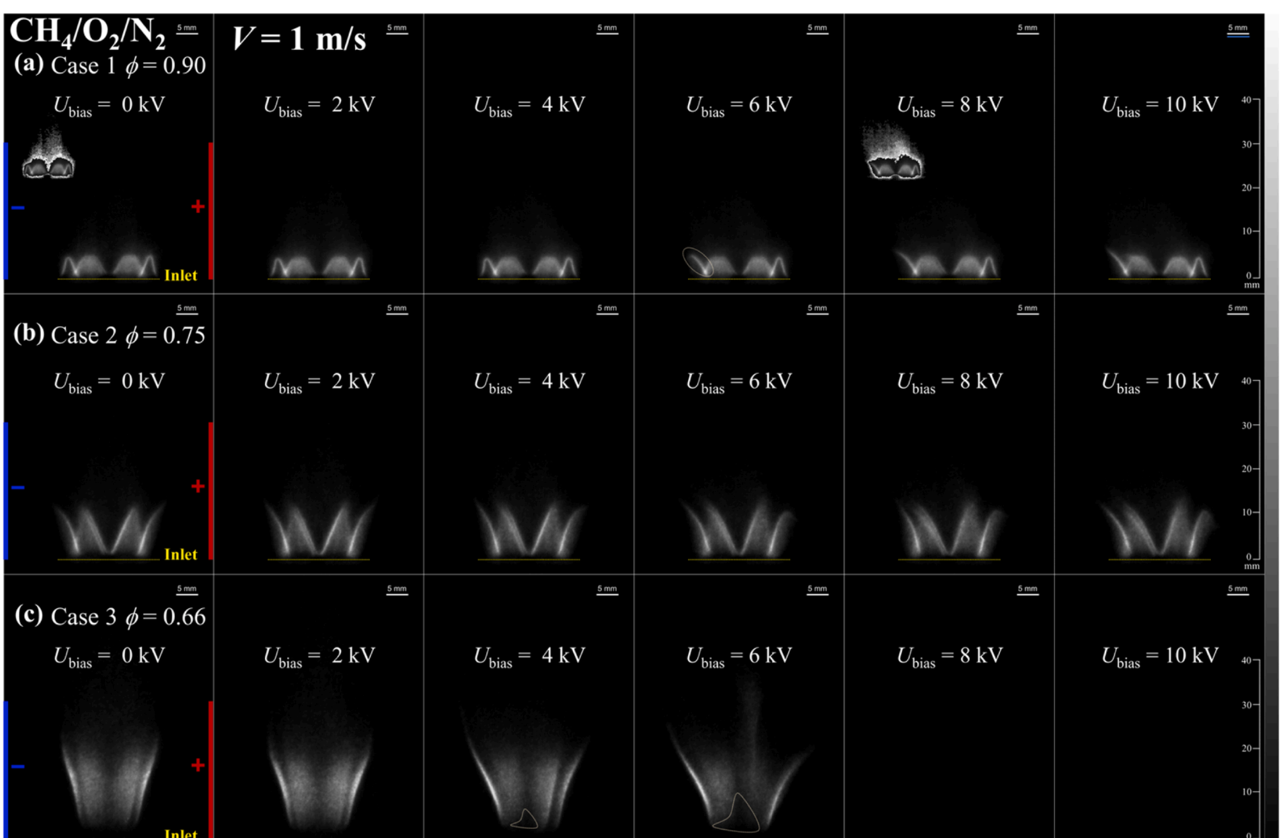

Fig. 6. The morphology of bluff body flames under the transverse DC electric field. (a) ϕ = 0.90; (b) ϕ = 0.75; (c) ϕ = 0.66.

side in the transverse DC electric field with a high bias voltage, as is shown in Fig. 6(b). Moreover, in Fig. 6(c), an extinction of lifting bluff body flames at $\phi = 0.66$, which have a relatively low adiabatic flame temperature (T_a) and laminar burning velocity (S_L), is observed in the transverse DC electric field at $U_{bias} \geq 8$ kV. Simultaneously, varying degrees of localized quenching occurs in the root of bluff body flames at $U_{bias} = 4$ kV and 6 kV. In particular, it is observed that the flame perturbation is exacerbated under a high bias voltage which is probably relevant to the flame instability, especially in lifting flames at $\phi = 0.66$. Fig. 7 depicts the intensity of self-luminescence at different heights above the inlet with and without the effect of the transverse DC electric field. The morphological transition, from attachment to partial attachment, takes place at a distance of 10 mm from the central axis, as is illustrated in the Fig. 7(a) and Fig. 7(b). For partial attachment flames at $\phi = 0.75$, compared Fig. 7(d) with Fig. 7(e), the intensity of self-luminescence relatively increases on the left side while decreases on the right side in the transverse DC electric field, which is more noticeable in the lifting flame, as is depicted in Fig. 7(g) and Fig. 7(h). Furthermore, as to lifting flames at $\phi = 0.66$, it is observed a lower level of self-luminous intensity near the central axis at the height of <12 mm which corresponds to the localized quenching region. As a result, due to the ionic wind, a high-intensity transverse DC electric field intensifies the transition of flame morphology, such as from attachment to partial attachment, then to lifting, and finally to blow out. Fig. 7(c), Fig. 7(f), and Fig. 7(i) show the sumation of self-luminous intensities on the left and right sides of the central axis with and without the electric field, normalized by dividing by a constant value of 9000. The transverse electric field significantly alters flame symmetry at $\phi = 0.66$.

Except for the self-luminescence of flames, CH* and OH* emission signals are recorded using narrow bandwidth interference filters centered at 431 ± 10 nm and 307 ± 10 nm, respectively, to capture chemiluminescence from excited radicals. Chemiluminescence is generated due to the fact that the return of excited radicals formed in the flame front, such as CH* and OH*, from the excited energy state to a lower energy state, will be accompanied by the emission of light at a characteristic wavelength. Literature studies suggest that the chemiluminescent intensity of radicals may be a good marker for the heat release and front of premixed flames [50]. Chemiluminescence has been extensively studied as a combustion diagnostic method evaluating the flame structure, extinction, chemical reaction, and heat release [51–54]. The distributions of CH* and OH*radicals are altered by the transverse DC electric field, as is depicted in Fig. 8. According to the signals of radical emissions, OH* radicals are smoother compared with the CH* radicals. Similarly, the transition in flame structures at $\phi = 0.90$, from attachment to partial attachment, occur at $U_{bias} = 6$ kV. Fig. 9 shows the emission intensity of CH* and OH*radicals in lifting flames at different heights with and without the effect of the transverse DC electric field. Fig. 9(c) and Fig. 9(f) show the sumation of CH* and OH* emission instensity on the left and right sides of the central axis with and without the electric field, normalized by dividing by a constant value of 9000. For the lifting flames at $\phi = 0.66$, the intensity of CH* and OH* emissions near the central axis approaches the zero value over different heights, which are attributable to localized quenching. Besides, the emission level of radicals on the negative electrode side is greater than that on the positive electrode side under the transverse DC electric field, which may be attributed to the transverse movement of radicals is accelerated by the electric field. Furthermore, the longitudinal distribution of radicals is also changed by the transverse DC electric field. The height of the maximum emission profile of OH* appears at 12 mm and 9 mm without and with the electric field, respectively.

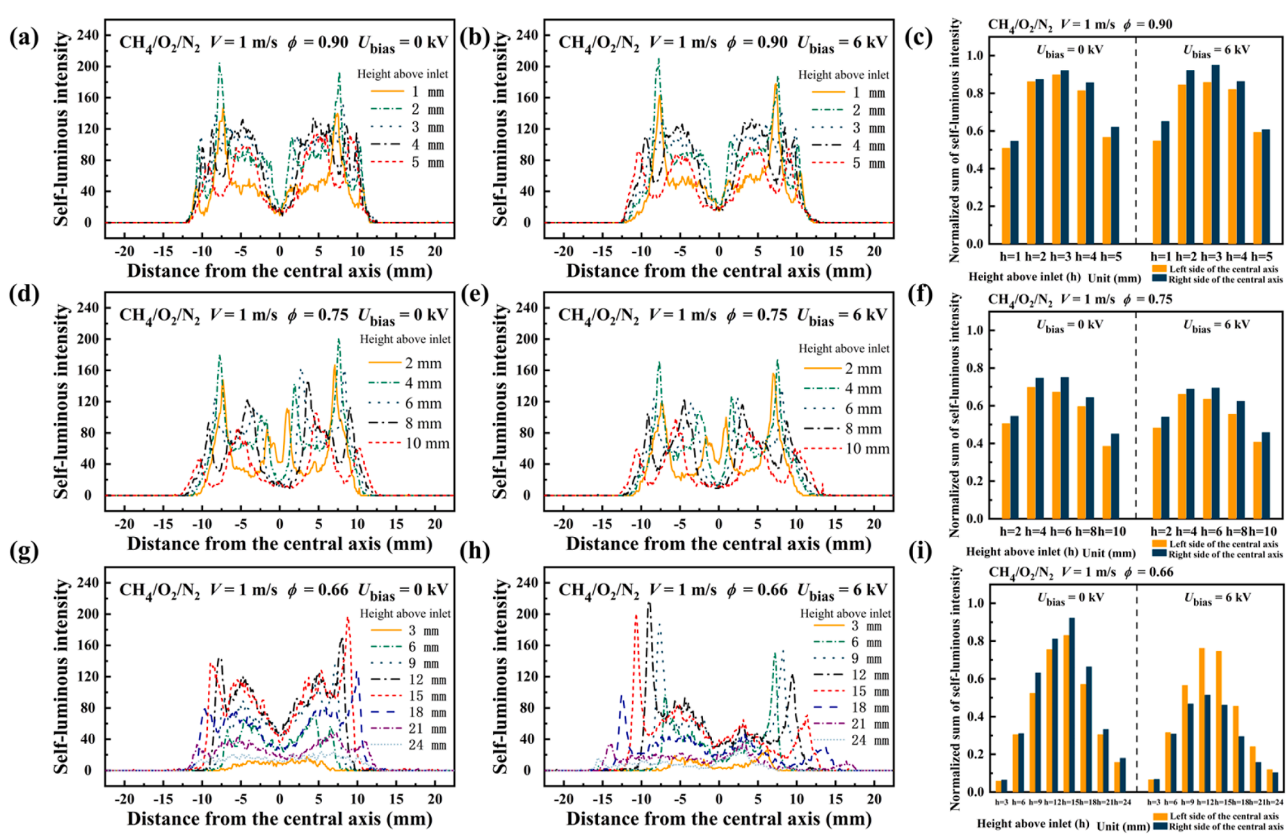

Fig. 7. Comparisons of self-luminous intensity at different heights with and without the transverse DC electric field. (a) $\phi = 0.90$, $U_{bias} = 0$ kV; (b) $\phi = 0.90$, $U_{bias} = 6$ kV; (c) Normalized sumation of self-luminous intensity, $\phi = 0.90$; (d) $\phi = 0.75$, $U_{bias} = 0$ kV; (e) $\phi = 0.75$, $U_{bias} = 6$ kV; (f) Normalized sumation of self-luminous intensity, $\phi = 0.75$; (g) $\phi = 0.66$, $U_{bias} = 0$ kV; (h) $\phi = 0.66$, $U_{bias} = 6$ kV; (i) Normalized sumation of self-luminous intensity, $\phi = 0.66$.

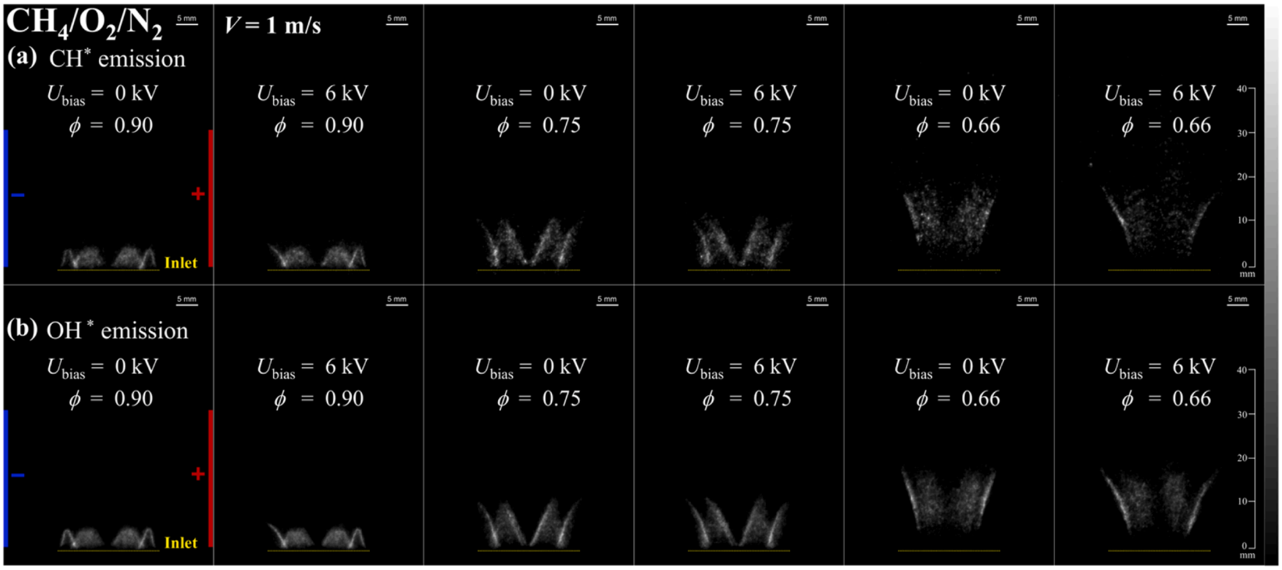

Fig. 8. Signals of CH* and OH* emissions with and without the transverse DC electric field. (a) CH* emissions; (b) OH* emissions.

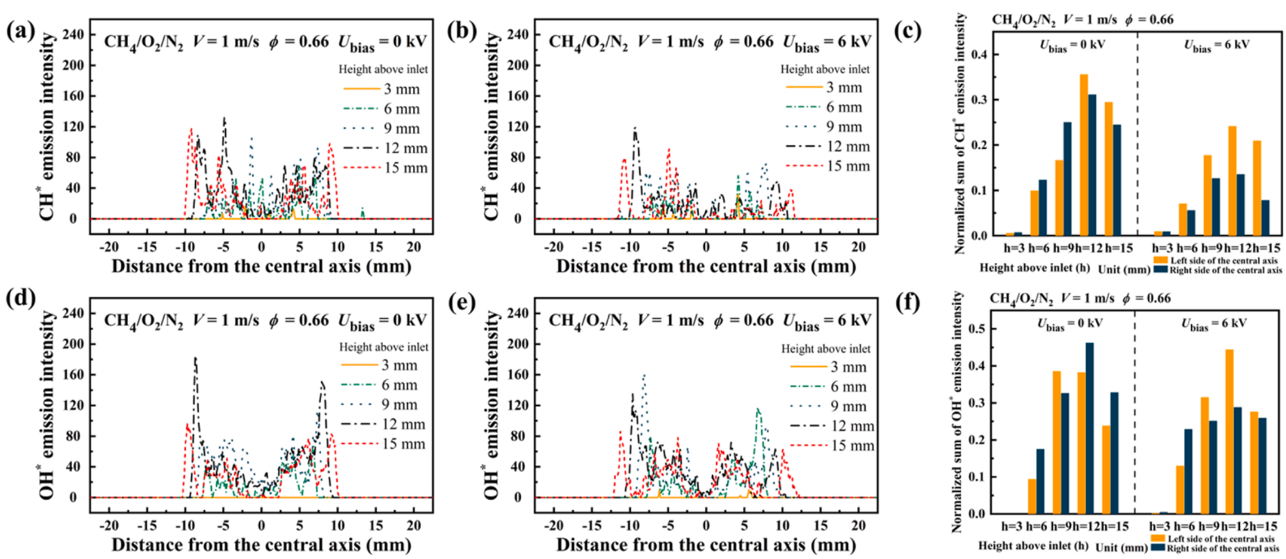

Fig. 9. Comparisons of the emissions intensity of CH* and OH* at different heights with and without the transverse DC electric field. (a) $\phi = 0.66$, $U_{bias} = 0$ kV, CH* emissions; (b) $\phi = 0.66$, $U_{bias} = 6$ kV, CH* emissions; (c) Normalized sumation of CH* emissions intensity, $\phi = 0.66$; (d) $\phi = 0.66$, $U_{bias} = 0$ kV, OH* emissions; (e) $\phi = 0.66$, $U_{bias} = 6$ kV, OH* emissions; (f) Normalized sumation of OH* emissions intensity, $\phi = 0.66$.

3.3. Analysis of extinction induced by the transverse DC electric field

Experimental observations in this study indicate that a high-intensity ($U_{bias} \geq 8$ kV) transverse DC electric field can induce the extinction of the bluff body flame at $\phi = 0.66$ or in the lifting morphology. The ionic wind, resulting from the electric body force on charged species in the transverse DC electric field, significantly enhances flow momentum [10, 49]. Furthermore, the ionic wind effect exacerbates the transition of flame morphologies and the tendency to blow out, particularly near the negative electrode side, indicating that positive ions predominantly drive the ionic wind. Besides, the lifting flame approaching extinction exhibit strong perturbations and distortions of the flame front under a high-intensity transverse DC electric field.

To clarify probable explanations for the morphological transformation and extinction of bluff body flames induced by the transverse DC electric field, a further flame experiment has been designed by using the CO_2 dilution. The specific experimental conditions are listed in

Table 2
Experimental conditions (different Lewis numbers).

Mixture	V (m/s)	ϕ	x (%)	β	U_{bias} (kV)	Le	T_a (K)
$CH_4/O_2/N_2/CO_2$	1	0.90	0 - 50	1.0 - 0.74	0	1.0 - 0.802	2139
$CH_4/O_2/N_2/CO_2$	1	0.75	0 - 50	1.0 - 0.76	0	1.0 - 0.796	1924
$CH_4/O_2/N_2/CO_2$	1	0.66	0 - 50	1.0 - 0.77	0	1.0 - 0.793	1775
$CH_4/O_2/N_2/CO_2$	1	0.66	10	0.95	4	0.950	1775
$CH_4/O_2/N_2/CO_2$	1	0.60 - 0.90	0 - 50	1.0 - 0.74	8	1.0 - 0.790	1669 - 2139

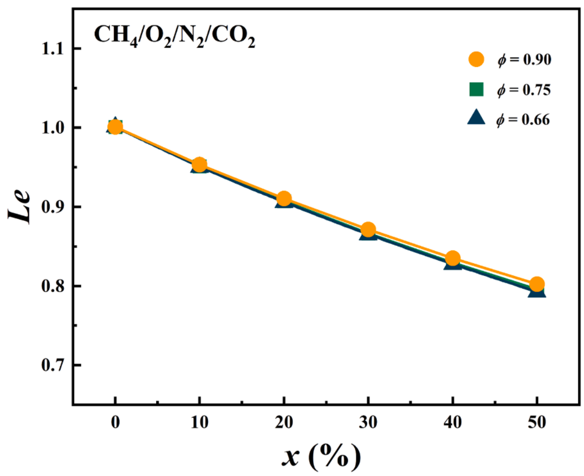

Fig. 10. Variations of the Lewis number with the blending ratio of CO_2 at different equivalence radios.

Table 2. Fig. 10 shows the variation of Le with x for the $CH_4/O_2/N_2/CO_2$ mixture at different ϕ. Replacing a partial N_2 dilution by CO_2 drops the Le of mixture down to below the unity at various ϕ. The thermal diffusive instability, as an inherent instability of flames, occurs where $Le < 1$.

Images of the bluff body flames at different x are depicted in Fig. 11. The height of bluff body flames increases as x grows for different flame morphologies. In Fig. 11(b), the lifting phenomenon is observed for partially attached flames at $x \geq 40$ %, which can be attributed to the fact that the replacement of the diluent by CO_2 reduces the S_L of the mixture. Furthermore, for the lifting flames at $\phi = 0.66$ and $V = 1$ m/s, the flames undergo wrinkling to varying degrees and a distinct distortion of the flame outlines is observed at $x \geq 20$ % or $Le < 0.91$ as depicted in Fig. 11 (c). Consequently, the thermal diffusion instability exacerbates the flame wrinkling leading to enhanced perturbation of the front of bluff body flames.

The experiments above clearly exhibit the evolution of thermal diffusive instability with CO_2 additions or reduce Le and without transverse DC electric field. Furthermore, to elaborate the kinetic effect of transverse DC electric field on the bluff body flame instability, the transient experiment of $CH_4/O_2/N_2/CO_2$ lifting flame within 40 ms at $x = 10$ %, $\phi = 0.66$, $V = 1$ m/s, and $Le \approx 1.0$ without a transverse DC electric field, where thermal diffusive instability does not take place, is compared with the same mixture in a transverse DC electric field in Fig. 12. The relevant video of transient evolutions of flame instability is attached in the supplementary material. Under the presence of a transverse DC electric field, the perturbation of the flame front is exacerbated and a visible distortion of the outline is observed, which is consistent with the behavior of the lifting flames in thermal diffusive instabilities without the transverse DC field at $x \geq 20$ %. The transverse DC electric field makes the visible distortion to be advanced at a lower x or lower CO_2 additions, which indicates that the flame wrinkles and distortions in relation to the thermal diffusive instability are intensified. Further, the strong disturbance of the flame front hastens the extinction of bluff body flames. It implies that the extinction of bluff body flames under $\phi = 0.66$ and $U_{bias} \geq 8$ kV in Fig. 6(c) is probably because of both the ionic wind and thermal diffusive instability induced by the transverse DC electric field.

Fig. 13 depicts the ionic current, I, as a function of U_{bias} under varying inlet conditions. I is shown to increase with U_{bias}, indicating enhanced ion mobility and charge transport as the electric field intensifies. This trend supports the observed ionic wind effect where the electric body force on charged species amplifies flow momentum, contributing to flame front perturbations and morphological transitions

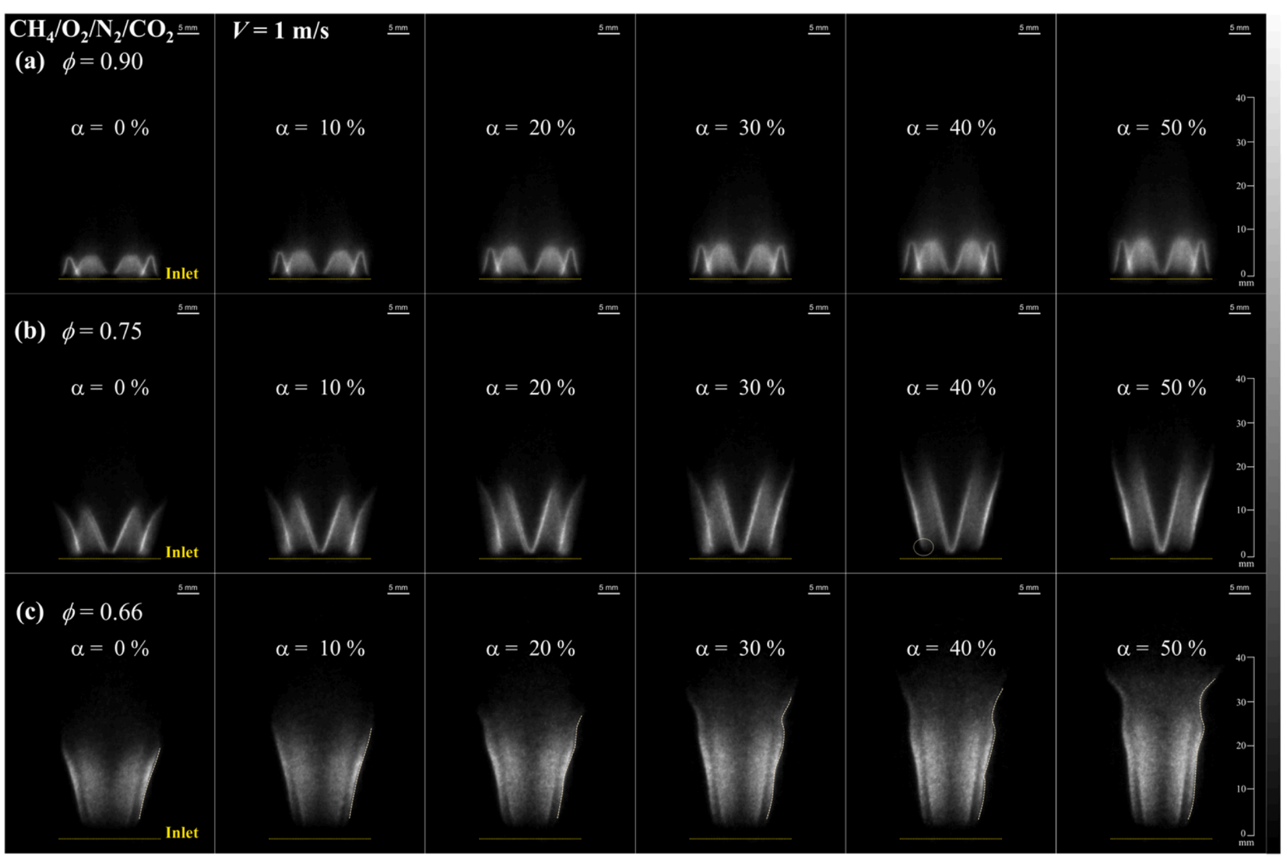

Fig. 11. Direct high-speed images of bluff body flames at different blending ratios of CO_2. (a) $\phi = 0.90$; (b) $\phi = 0.75$; (c) $\phi = 0.66$.

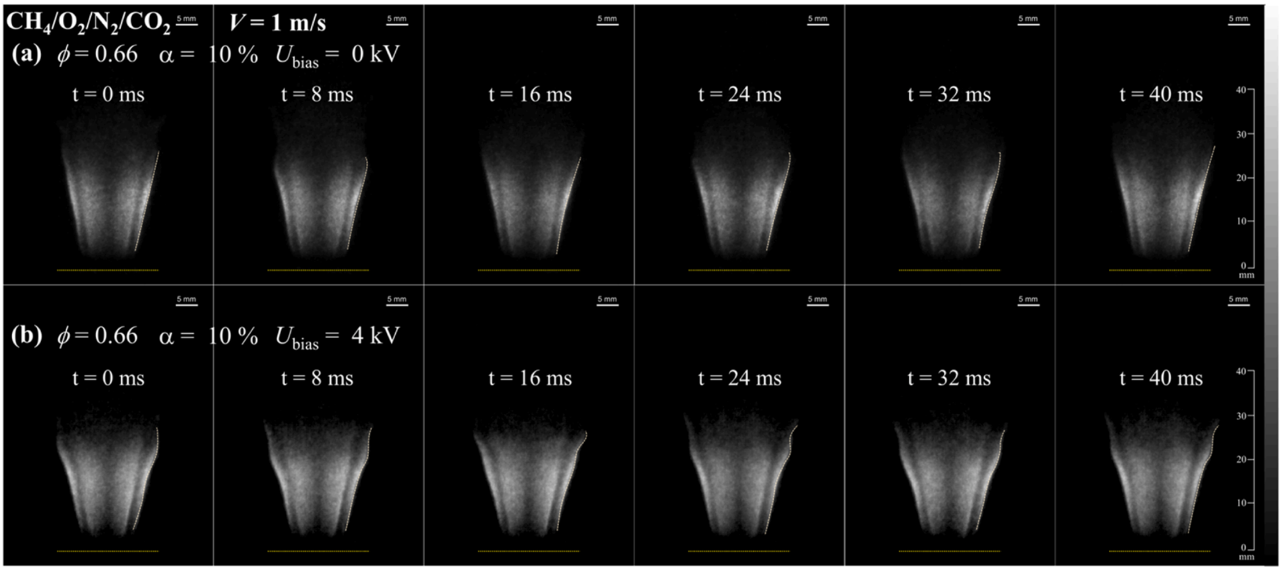

Fig. 12. Direct high-speed transient images of bluff body flames without and with a transverse electric field. (a) $U_{bias} = 0$ kV; (b) $U_{bias} = 4$ kV.

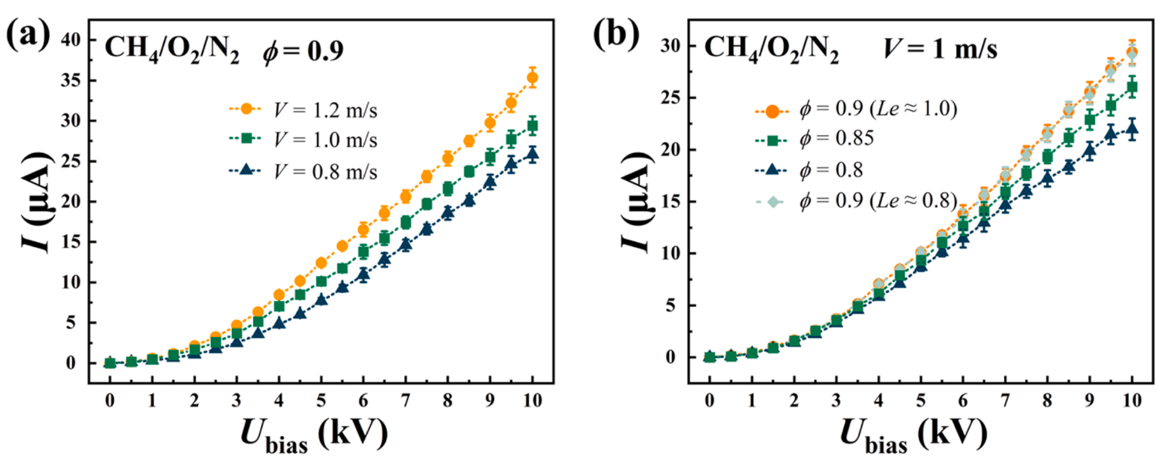

Fig. 13. Ionic current as a function of bias voltage under different inlet conditions. (a) varying V; (b) varying ϕ and Le.

as depicted in Fig. 6. Higher ϕ and V lead to increased ionic current due to enhanced charged species density. Importantly, when the V and ϕ are held constant, variations in Le result in only marginal changes in ionic current. This suggests that the density of charged species in the flame is not significantly altered by changes in Le under the conditions tested.

In addition to the two-dimensional high-speed images, extinction experiments induced by the transverse DC electric field are implemented at different x, as is depicted in Fig. 14. In present experiments, a ramping rate of 25 kV/min is uniformly adopted to eliminate the effect of the boosting rate of the high-voltage DC source. The adiabatic flame temperature, T_a, is controlled to be identical in the CO_2 dilution experiments, hence minimizing the influence of the replacement of N_2 by CO_2 on S_L, which has a slight slowdown with increasing x. The results show that the CO_2-diluted or $Le < 1$ bluff body flames are more likely to exhibit a tendency to the extinction at a lower bias voltage. Specifically, the extinction happens at approximately $U_{bias} = 8$ kV for bluff body flames without CO_2 dilution or without significant thermal diffusive instability ($x = 0$ % or $Le = 1.0$), whereas happens at approximately $U_{bias} = 4$ kV with CO_2 dilution or with significant thermal diffusive instability ($Le = 0.79$ or $x = 50$ %). Simultaneously, the bias voltage of the extinction presents a nonlinearity decrease with the increase in x.

Extinction experiments are conducted to determine the effects of ϕ and Le under $V = 1$ m/s and $U_{bias} = 8$ kV, as depicted in Fig. 15. The results reveal that for $\phi > 0.75$ and $Le > 0.79$ ($x = 50$ %), bluff body flames remain stable and do not extinguish, even at high bias voltages. This threshold behavior underscores the critical role of ϕ and Le in

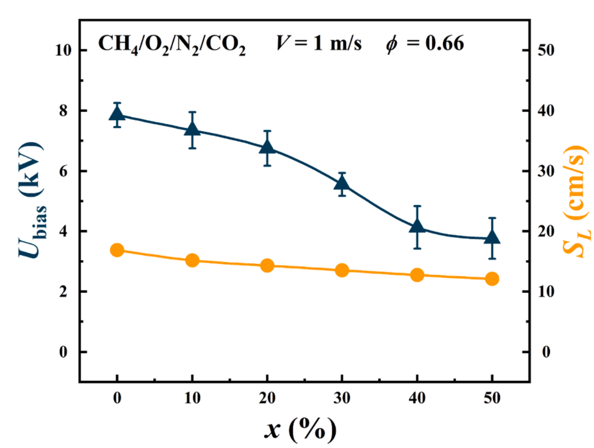

Fig. 14. Variations of the bias voltage of extinction and laminar burning velocities with the blending ratios of CO_2.

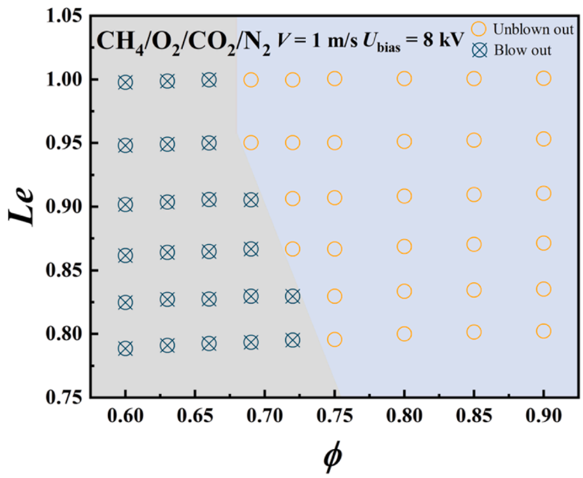

Fig. 15. Extinction characteristics of the bluff body flame at different ϕ and Le under $V = 1$ m/s and $U_{bias} = 8$ kV.

modulating flame stability, with richer mixtures demonstrating enhanced resistance to extinction due to increased flame strength.

The extinction is governed by multiple dimensionless parameters, including Re, ϕ, and Le, which collectively determine the balance between chemical reaction rates and transport processes. Previous have shown that Re influences extinction by altering mixing and heat transfer, while ϕ affects flame temperature and reaction rates, with lean mixtures being more prone to extinction due to reduced heat release. The present study identifies the extinction mechanism driven by electric field induced modification of Le. The Lewis number of the combustion mixture is highly relevant to the mass diffusion of radicals and ions (instead of diluents), which are high reactive but in low concentrations at highly diluted fuel lean conditions. The elevated electric field strength leads to a significant decrease in the Lewis number. Once the Lewis number is lower than unity with increasing the electric field strength, and then the flame wrinkles and disturbances are exacerbated, eventually accelerating the extinction. The present research reveals the effect of transverse electric field on extinction and aids to adjust flame instabilities by using a proper electric field.

4. Conclusions

Understanding the coupling mechanisms between electric fields and flame instability or extinction is crucial for addressing challenges in practical burner applications, such as combustion stability, flame extinction, and safety concerns. In this work, the effect of the transverse DC electric field on bluff body flames is experimentally investigated. The flame morphology, including attachment, partial attachment, lifting, and blow out, are classified using a $CH_4/O_2/N_2$ premixed flame. It is seen that the high-intensity transverse DC electric field intensifies the flame morphology transition from attachment to partial attachment, then to lifting, and finally to blow out. This is attributed to increased flow momentum driven by ionic wind and enhanced flame instability caused by the transverse DC electric field.

To further explore the effect of the transverse DC electric field on flame extinction, experiments with CO_2-diluted laminar bluff body flame are conducted at varying Lewis numbers. For the lifting flame, it has been observed that thermal diffusive instability ($Le < 1$) leads to an exacerbated flame wrinkling and disturbances. In the case of a transverse DC electric field with a bias voltage of 4 kV, the visible flame distortions caused by thermal diffusive instabilities were observed for the $CH_4/O_2/CO_2/N_2$ mixture at $\phi = 0.66$, $V = 1$ m/s, and $Le \approx 1.0$, which were not observed without the electric field. Meanwhile, the bias voltage for the extinction of bluff body flames decreases with a decrease in Lewis numbers or an increase in blending ratios of CO_2.

This work elucidates the impact of a transverse DC electric field on the extinction of bluff body flames under elevated electric field strengths. On the one hand, the transverse electric field facilitates the morphological transition of bluff body flames through the ions wind. On the other hand, the transverse electric field exacerbates the thermal diffusive instability, and eventually leads to extinction.

Novelty and significance statement

The novelty of this study lies in systematically revealing the coupled mechanisms by which a transverse direct current (DC) electric field induces the extinction of laminar bluff body stabilized flames through both ionic wind effects and exacerbated thermal diffusive instability. High-intensity transverse DC electric fields dramatically accelerate morphological transitions and reduce the bias voltage required for extinction, especially at lower Lewis numbers. These findings uncover the synergistic interplay between electrophoretic (ionic wind) forcing and intrinsic flame instabilities under electric fields, providing critical physical insights for electric-field-based flame suppression strategies, active control of combustion instability in practical combustors.

CRediT authorship contribution statement

Bowen Liu: Writing – review & editing, Writing – original draft, Methodology, Conceptualization, Data curation. **Jianling Li:** Writing – review & editing, Methodology. **Yunke Wu:** Methodology, Supervision, Project administration. **Hao Zhao:** Writing – review & editing, Methodology, Supervision, Project administration.

Declaration of competing interest

The authors declare that they have no known competing financial interests or personal relationships that could have appeared to influence the work reported in this paper.

Acknowledgments

This work was supported by the National Natural Science Foundation of China (No. 22361132538). This work was also supported by National Natural Science Foundation of China - 'YE Qisun' Science Foundation Project (No. U2241255), the Advanced Jet Propulsion Innovation Center (No. ZZCX-2020-004), and the National Science and Technology Major Project (No. P2022-AB-II-005-003; No. J2019-III-0022-0066).

Supplementary materials

Supplementary material associated with this article can be found, in the online version, at doi:10.1016/j.combustflame.2025.114665.

References

[1] H. Liu, W. Cai, Recent progress in electric-field assisted combustion: a brief review, Front. Energy 16 (2021) 883–899.
[2] L. Zigan, Overview of electric field applications in energy and process engineering, Energies 11 (2018) 1361.
[3] M. Belhi, P. Domingo, P. Vervisch, Direct numerical simulation of the effect of an electric field on flame stability, Combust. Flame 157 (2010) 2286–2297.
[4] M.K. Kim, S.H. Chung, H.H. Kim, Effect of AC electric fields on the stabilization of premixed bunsen flames, Proc. Combust. Inst. 33 (2011) 1137–1144.
[5] M.K. Kim, S.K. Ryu, S.H. Won, S.H. Chung, Electric fields effect on liftoff and blowoff of nonpremixed laminar jet flames in a coflow, Combust. Flame 157 (2010) 17–24.
[6] R.I. Noorani, R.E. Holmes, Effects of electric fields on the blowoff limits of a methane-air flame, AIAA J 23 (1985) 1452–1454.
[7] A. Sayed-Kassem, A. Elorf, P. Gillon, M. Idir, B. Sarh, V. Gilard, Numerical modelling to study the effect of DC electric field on a laminar ethylene diffusion flame, Int. Commun. Heat Mass Transfer 122 (2021) 105167.
[8] H. Duan, X. Wu, T. Sun, B. Liu, J. Fang, C. Li, Z. Gao, Effects of electric field intensity and distribution on flame propagation speed of CH4/O2/N2 flames, Fuel 158 (2015) 807–815.

[9] X. Gao, Z. Gao, Z. Du, H. Zhang, Z. He, Effect of low-frequency alternating-current electric field parameters on laminar and turbulent flames of CH4/air mixture, Fuel 317 (2022) 121755.
[10] D.G. Park, S.H. Chung, M.S. Cha, Visualization of ionic wind in laminar jet flames, Combust. Flame. 184 (2017) 246–248.
[11] D. Wisman, S. Marcum, B. Ganguly, Electrical control of the thermodiffusive instability in premixed propane–air flames, Combust. Flame. 151 (2007) 639–648.
[12] Y. Xiong, D.A. Lacoste, S.H. Chung, M.S. Cha, Effects of DC electric fields on flickering and acoustic oscillations of an M-shape premixed flame, Flow Turbul. Combust. 109 (2022) 459–475.
[13] S.H. Won, M.S. Cha, C.S. Park, S.H. Chung, Effect of electric fields on reattachment and propagation speed of tribrachial flames in laminar coflow jets, Proc. Combust. Inst. 31 (2007) 963–970.
[14] Y. Luo, Y. Gan, X. Jiang, Investigation of the effect of DC electric field on a small ethanol diffusion flame, Fuel 188 (2017) 621–627.
[15] J.D.B.J. van den Boom, A.A. Konnov, A.M.H.H. Verhasselt, V.N. Kornilov, L.P.H. de Goey, H. Nijmeijer, The effect of a DC electric field on the laminar burning velocity of premixed methane/air flames, Proc. Combust. Inst. 32 (2009) 1237–1244.
[16] Y. Xiong, S.H. Chung, M.S. Cha, A parametric study of AC electric field-induced toroidal vortex formation in laminar nonpremixed coflow flames, Combust. Flame. 182 (2017) 142–149.
[17] Y. Luo, Y. Gan, J. Xu, Y. Yan, Y. Shi, Effects of electric field intensity and frequency of AC electric field on the small-scale ethanol diffusion flame behaviors, Appl. Therm. Eng. 115 (2017) 1330–1336.
[18] D.G. Park, S.H. Chung, M.S. Cha, Dynamic responses of counterflow nonpremixed flames to AC electric field, Combust. Flame. 198 (2018) 240–248.
[19] S.K. Ryu, Y.K. Kim, M.K. Kim, S.H. Won, S.H. Chung, Observation of multi-scale oscillation of laminar lifted flames with low-frequency AC electric fields, Combust. Flame. 157 (2010) 25–32.
[20] Y. Tang, M. Simeni Simeni, Q. Yao, I.V. Adamovich, Non-premixed counterflow methane flames in DC/AC/NS electric fields, Combust. Flame. 240 (2022) 112051.
[21] Y. Xiong, S.H. Chung, M.S. Cha, Instability and electrical response of small laminar coflow diffusion flames under AC electric fields: toroidal vortex formation and oscillating and spinning flames, Proc. Combust. Inst. 36 (2017) 1621–1628.
[22] F. Altendorfner, J. Kuhl, L. Zigan, A. Leipertz, Study of the influence of electric fields on flames using planar LIF and PIV techniques, Proc. Combust. Inst. 33 (2011) 3195–3201.
[23] J. Kuhl, T. Seeger, L. Zigan, S. Will, A. Leipertz, On the effect of ionic wind on structure and temperature of laminar premixed flames influenced by electric fields, Combust. Flame. 176 (2017) 391–399.
[24] Y. Ren, W. Cui, S. Li, Electrohydrodynamic instability of premixed flames under manipulations of dc electric fields, Phys. Rev. E. 97 (2018) 13103.
[25] A. Liu, K.H. Luo, S. Rigopoulos, W. Jones, Effects of the electric field on soot formation in combustion: a coupled charged particle PBE-CFD framework, Combust. Flame. 239 (2022) 111796.
[26] C. Guerra-Garcia, M. Martinez-Sanchez, Counterflow nonpremixed flame DC displacement under AC electric field, Combust. Flame. 162 (2015) 4254–4263.
[27] A. Ata, J.S. Cowart, A. Vranos, B.M. Cetegen, Effects of direct current electric field on the blowoff characteristics of bluff-body stabilized conical premixed flames, Combust. Sci. Technol. 177 (2005) 1291–1304.
[28] H.F. Calcote, R.N. %J I. Pease, Engineering chemistry, electrical properties of flames, BurnerFlames. Longitudin. Electric. Field. 43 (1951) 2726–2731.
[29] P. Salvador, K.G. Xu, Effects of DC electric fields on the combustion of a simplified multi-element injector, (2017).
[30] X. Meng, X. Wu, C. Kang, A. Tang, Z. Gao, Effects of direct-current (DC) electric fields on flame propagation and combustion characteristics of premixed CH_4 /O_2 /N_2 flames, Energy Fuel. 26 (2012) 6612–6620.
[31] E.V. Vega, K.Y. Lee, An experimental study on laminar CH4/O2/N2 premixed flames under an electric field, J. Mech. Sci. Technol. 22 (2008) 312–319.
[32] M. Sánchez-Sanz, D.C. Murphy, C. Fernandez-Pello, Effect of an external electric field on the propagation velocity of premixed flames, Proc. Combust. Inst. 35 (2015) 3463–3470.
[33] S. Kadowaki, T. Hasegawa, Numerical simulation of dynamics of premixed flames: flame instability and vortex–flame interaction, Prog. Energy Combust. Sci. 31 (2005) 193–241.
[34] N.I. Kim, U.D. Lee, H.D. Shin, Extinction of a premixed flame by a large variation in axial velocity, Combust. Flame. 136 (2004) 467–480.
[35] M. Matalon, Intrinsic flame instabilities in premixed and nonpremixed combustion, Annu. Rev. Fluid Mech. 39 (2007) 163–191.
[36] C.J. Sung, C.K. Law, Extinction mechanisms of near-limit premixed flames and extended limits of flammability, in: 1996: pp. 865–873.
[37] Y. Wang, S. Hu, R.W. Pitz, Extinction and cellular instability of premixed tubular flames, Proc. Combust. Inst. 32 (2009) 1141–1147.
[38] P. Clavin, Dynamic behavior of premixed flame fronts in laminar and turbulent flows, Prog. Energy Combust. Sci. 11 (1985) 1–59.
[39] G.H. Markstein, Experimental and theoretical studies of flame-front stability, J. Aeronaut. Sci. 18 (1951) 199–209.
[40] G.I. Sivashinsky, Diffusional-thermal theory of cellular flames, Combust. Sci. Technol. 15 (1977) 137–145.
[41] L. Berger, A. Attili, H. Pitsch, Intrinsic instabilities in premixed hydrogen flames: parametric variation of pressure, equivalence ratio, and temperature. Part 2 – non-linear regime and flame speed enhancement, Combust. Flame. 240 (2022) 111936.
[42] S. Zhao, B. Liu, B. Zhao, T. Li, Q. Shu, Numerical simulation of ethanol air diffusion flame quenching under transverse AC electric field, Fire 5 (2022) 196.
[43] E. Sher, G. Pinhasi, A. Pokryvailo, Extinction of pool flames by means of a DC electric field, Combust. Flame. 94 (1993) 244–252.
[44] A. Sakhrieh, G. Lins, F. Dinkelacker, T. Hammer, A. Leipertz, D.W. Branston, The influence of pressure on the control of premixed turbulent flames using an electric field, Combust. Flame. 143 (2005) 313–322.
[45] S. Marcum, B. Ganguly, Electric-field-induced flame speed modification, Combust. Flame. 143 (2005) 27–36.
[46] S. Zitouni, D. Pugh, A. Crayford, P.J. Bowen, J. Runyon, Lewis number effects on lean premixed combustion characteristics of multi-component fuel blends, Combust. Flame. 238 (2022) 111932.
[47] A.J. Fillo, J. Schlup, G. Beardsell, G. Blanquart, K.E. Niemeyer, A fast, low-memory, and stable algorithm for implementing multicomponent transport in direct numerical simulations, J. Comput. Phys. 406 (2020) 109185.
[48] F. Altendorfner, F. Beyrau, A. Leipertz, T. Hammer, D. Most, G. Lins, D. W. Branston, Technical feasibility of electric field control for turbulent premixed flames, Chem. Eng. Amp; Technol. 33 (2010) 647–653.
[49] M. Belhi, B.J. Lee, M.S. Cha, H.G. Im, Three-dimensional simulation of ionic wind in a laminar premixed bunsen flame subjected to a transverse DC electric field, Combust. Flame 202 (2019) 90–106.
[50] I.R. Hurle, R.B. Price, T.M. Sugden, A. Thomas, Sound emission from open turbulent premixed flames, Proc. R. Soc. London, Ser. A. 303 (1968) 409–427.
[51] N. Denisova, P. Tretyakov, A. Tupikin, Emission tomography in flame diagnostics, Combust. Flame. 160 (2013) 577–588.
[52] T. García-Armingol, J. Ballester, Flame chemiluminescence in premixed combustion of hydrogen-enriched fuels, Int. J. Hydrogen Energy. 39 (2014) 11299–11307.
[53] Y. Hardalupas, M. Orain, Local measurements of the time-dependent heat release rate and equivalence ratio using chemiluminescent emission from a flame, Combust. Flame. 139 (2004) 188–207.
[54] J. Kojima, Y. Ikeda, T. Nakajima, Basic aspects of OH(a), CH(a), and C2(d) chemiluminescence in the reaction zone of laminar methane–air premixed flames, Combust. Flame. 140 (2005) 34–45.